Sensors and Materials, Vol. 37, No. 11 (2025) 5071–5079
MYU Tokyo

S & M 4233

Effect of Nanoparticle Size on the Photovoltaic Performance of Sol–gel-derived TiO_2 Thin-film Dye-sensitized Solar Cells

Ming-Cheng Kao,[1*] Kai-Huang Chen,[2**] and Cheng-Shu Hsiao[3]

[1]Graduate Institute of Aeronautics, Department of Information and Communication Engineering, Chaoyang University of Technology, Taichung 413310, Taiwan
[2]Department of Electronic Engineering, Cheng Shiu University, Kaohsiung 83347, Taiwan
[3]Institute of Applied Information Technology, Ling Tung University, Taichung 413310, Taiwan;

(Received June 5, 2025; accepted November 18, 2025)

Keywords: TiO_2, nanoparticle, sol–gel, DSSC

In this study, a TiO_2 precursor solution was synthesized by the sol–gel method, and TiO_2 nanoparticles of different sizes (5, 25, 32, and 100 nm) were added to investigate their effects on the properties of dye-sensitized solar cells (DSSCs). Thin films were deposited onto fluorine-doped tin oxide substrates via spin coating and subsequently sintered at 600 °C. The effects of nanoparticle size on the surface morphology, optical characteristics, and photovoltaic performance of the resulting DSSCs were systematically studied. X-ray diffraction (XRD) was employed for structural analysis, while UV–VIS–NIR spectroscopy was used to measure the optical transmittance and absorbance of the films. The surface and cross-sectional morphology, grain size, and film thickness were examined by scanning electron microscopy (SEM). The current–voltage characteristics and conversion efficiency of the DSSCs were evaluated under simulated sunlight using a solar simulator. The experimental results revealed that smaller TiO_2 nanoparticles generally led to improved photovoltaic performance. However, the film fabricated with 5 nm nanoparticles exhibited significant surface aggregation, which adversely affected the short-circuit current density (J_{sc}) and conversion efficiency, compared with the film fabricated with 25 nm nanoparticles. Among all the samples, the DSSC based on 25 nm TiO_2 nanoparticles showed the best performance, featuring a uniform and smooth film morphology, J_{sc} of 14.49 mA/cm^2, and a conversion efficiency of 6.05%.

1. Introduction

Dye-sensitized solar cells (DSSCs), as a promising third-generation photovoltaic technology, have attracted extensive attention over the past two decades because of their low fabrication cost, environmental friendliness, and compatibility with flexible substrates.[1–3] Unlike conventional silicon-based solar cells, DSSCs operate by means of a photoelectrochemical mechanism in which dye molecules absorb light and then inject electrons into a wide-bandgap semiconductor such as titanium dioxide (TiO_2). The efficiency of this process depends largely on the surface

*Corresponding author: e-mail: kmc@cyut.edu.tw
**Corresponding author: e-mail: 5977@csu.edu.tw
https://doi.org/10.18494/SAM5778

ISSN 0914-4935
https://myukk.org/

area, crystallinity, and electron transport properties of the TiO_2 layer.[4–6] TiO_2 is widely used in DSSCs owing to its excellent chemical stability, proper band alignment with dye molecules, and relatively low cost.[7–10] Among the various synthetic methods for preparing TiO_2 photoanodes, the sol–gel method is popular because of its simplicity, cost-effectiveness, and good control over the stoichiometry and morphology of the resulting films.[11–15] However, pure sol–gel-derived TiO_2 films usually have low surface roughness and limited surface area, which restricts dye adsorption and limits light harvesting efficiency.[16–18]

Researchers have incorporated TiO_2 nanoparticles into the sol–gel matrix to enhance the porosity and specific surface area of the photoanode.[19–21] The addition of nanoparticles not only increases the dye loading capacity but also changes the electron transport network within the film. Although several studies on different TiO_2 morphologies, such as nanorods, nanotubes, and mesoporous structures, have been carried out, few research groups have systematically investigated the effect of nanoparticle size on TiO_2 thin films prepared by the sol–gel method. Furthermore, the size of the nanoparticles can significantly affect the key properties of the photoanode. Therefore, studying the optimal particle size for these effects is crucial to improve the overall DSSC efficiency.

In this study, TiO_2 nanoparticles of four different sizes (5, 25, 32, and 100 nm) were added to the sol–gel-derived TiO_2 precursor solution. The thin films were deposited on fluorine-doped tin oxide (FTO) substrates by a sol–gel method. The effects of nanoparticle size on the surface morphology, optical transmittance, and photovoltaic performance of the resulting DSSCs were systematically investigated. Characterization was performed by X-ray diffraction (XRD), UV-visible-NIR spectroscopy, and scanning electron microscopy (SEM), while current–voltage (*I*–*V*) characteristics and power conversion efficiency were measured under simulated solar radiation.

2. Materials and Methods

Titanium (IV) isopropoxide (TTIP, 97%, Sigma-Aldrich) was used as the titanium source, and 2-methoxyethanol (99%, Alfa) was used as the solvent for the sol–gel process. The mixture was magnetically stirred for 2 h at 60 ℃ to form a homogeneous TiO_2 solution. 1 wt% TiO_2 nanoparticles with sizes of 5, 25, 32, and 100 nm were incorporated into the TiO_2 solution. A fluorine-doped tin oxide (FTO)-coated glass substrate (sheet resistance: ~10 Ω/sq) was used as a transparent conductive substrate. The TiO_2 solution was deposited by spin coating, followed by drying on a hotplate at 300 ℃. The obtained multilayer TiO_2 films were further processed using a rapid thermal annealing (RTA) system. The samples were heated to 600 ℃ at a rate of 100 ℃/min and kept at this temperature for 2 min to achieve crystallization and grain growth. Figure 1 shows representative photographs of TiO_2 films prepared with different nanoparticle sizes.

The annealed TiO_2 films were immersed in 0.5 mM N719 dye ethanol solution and sensitized in the dark at room temperature for 24 h. The electrodes were prepared by the dropwise addition of 10 mM chloroplatinic acid solution in isopropanol onto a clean FTO substrate. The DSSC device was assembled by sandwiching the dye-coated photoanode and platinum counter electrode using 60 μm Surlyn spacers (Solaronix) and injecting the iodide/triiodide electrolyte.

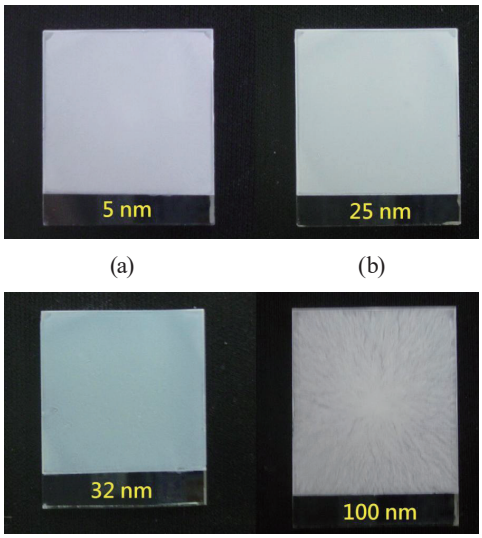

Fig. 1. (Color online) Sample photographs of sol–gel-derived TiO_2 thin films with nanoparticle sizes of (a) 5, (b) 25, (c) 32, and (d) 100 nm.

The crystal structure of the films was analyzed by XRD (Cu-Kα radiation, λ = 1.5406 Å). Optical transmittance and absorbance were measured by a UV–visible–near-infrared spectrometer (JASCO V-670). Field emission scanning electron microscopy (JEOL JSM-7600F) was used to characterize the surface and cross-sectional morphologies. The *I–V* characteristics of the DSSC were measured under simulated AM 1.5G sunlight (100 mW/cm^2) using a solar simulator (Newport 91160A) and a source meter (Keithley 2400). Figure 2 shows the structure and operation mechanism of the DSSC.

3. Results and Discussion

The crystal structures of films with different nanoparticle sizes (5, 25, 32, and 100 nm) were analyzed by XRD, and the results are shown in Fig. 3. All spectra show characteristic diffraction peaks corresponding to the anatase (A) or rutile (R) phase of TiO_2. Among all samples, the film with 25 nm TiO_2 nanoparticles showed the strongest anatase (101) diffraction peak at around 25.3° and a relatively weak rutile (110) peak at around 27.4°. This shows thatsuch a film has the highest anatase phase content and the lowest rutile phase content. The anatase phase has a higher conduction band edge, a lower charge recombination rate, and a higher dye affinity than the rutitle phase, making it more suitable for electron injection and dye adsorption in DSSC applications. It has been reported that TiO_2 with the anatase phase exhibits excellent electron transport properties and better photocatalytic activity owing to its good crystal structure and surface energy.[22] Therefore, TiO_2 thin films with 25 nm nanoparticles have the optimal anatase crystal phase composition, which can improve charge collection, reduce recombination, and increase the overall efficiency of the DSSC.

Figure 4 shows the top-view SEM images of TiO_2 thin films with nanoparticles of different particle sizes (5, 25, 32, and 100 nm). All films were annealed under rapid thermal annealing

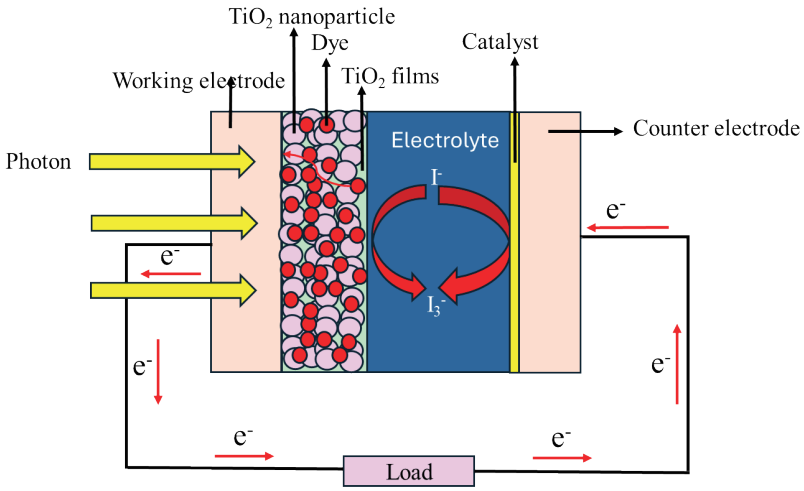

Fig. 2. (Color online) Schematic structure and operation mechanism of the dye-sensitized solar cell. The photoanode consists of a mesoporous TiO_2 layer sensitized with dye molecules.

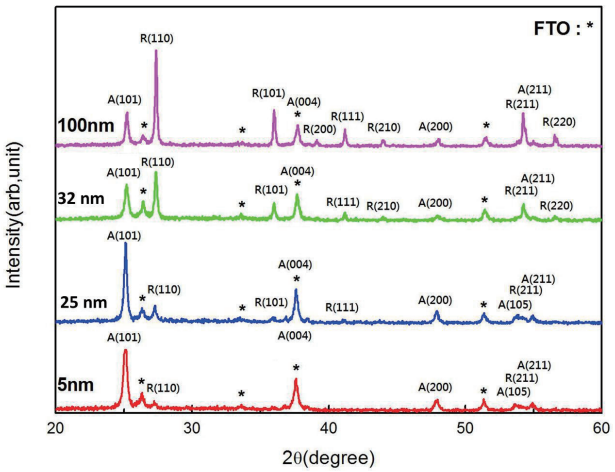

Fig. 3. (Color online) X-ray diffraction patterns for TiO_2 thin films with nanoparticle sizes of 5, 25, 32, and 100 nm. (A: anatase phase; R: rutile phase).

(RTA) at 600 °C. The surface morphology of the TiO_2 thin film with 5 nm nanoparticles showed obvious aggregation and grain clusters resulting in an uneven particle distribution. The TiO_2 thin film film with 25 nm nanoparticles exhibited a rough surface, a more uniform grain size, and an uneven grain distribution, as depicted in Fig. 4(b). The surface morphology of the TiO_2 thin film with 32 nm nanoparticles was similar to that of the film with 25 nm nanoparticles. However, the surface morphology of the film with 100 nm nanoparticles showed agglomeration, indicating that this particle size was very large, resulting in an uneven particle distribution.

Figure 5 shows the cross-sectional SEM images of the films with different nanoparticle sizes (5, 25, 32, and 100 nm). The film with 5 nm nanoparticles has a thickness of about 2.46 μm and an uneven surface, which may be due to the aggregation of finer particles. The film with 25 nm nanoparticles has a uniform structure, with a measured thickness of about 3.40 μm. The film

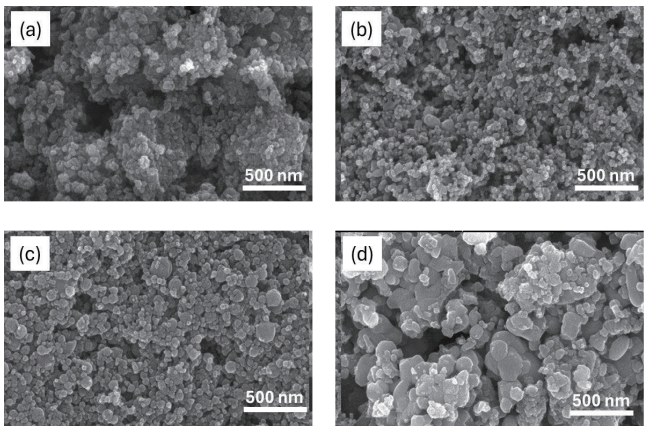

Fig. 4. Plane SEM images of TiO_2 thin films nanoparticle sizes of (a) 5, (b) 25, (c) 32, and (d) 100 nm.

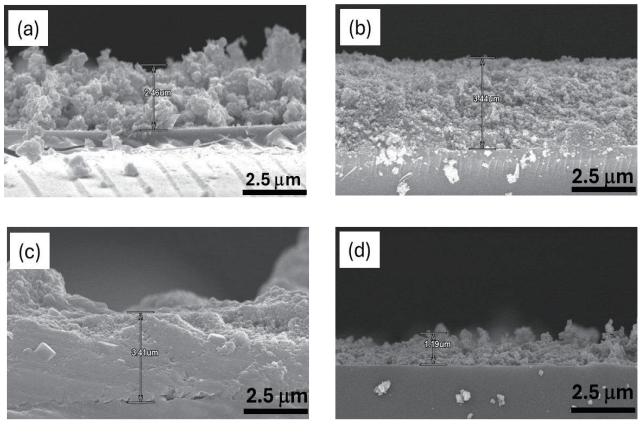

Fig. 5. Cross-sectional SEM images of TiO_2 thin films with nanoparticle sizes of (a) 5, (b) 25, (c) 32, and (d) 100 nm.

with 32 nm nanoparticles has a thickness of about 3.15 μm and an uneven surface. The film with 100 nm nanoparticles has the thinnest layer (about 1.19 μm) and a loose structure, which may be due to its larger nanoparticle size. In addition, the specific surface area and the amount of dye adsorbed on the surface of the TiO_2 thin films were further evaluated by Brunauer–Emmett–Teller (BET) analysis. By analyzing the BET surface area and dye adsorption capacity, the optimal nanoparticle size for achieving the highest dye-loading performance can be identified. Table 1 shows the relationship between nanoparticle size, specific surface area, and the amount of adsorbed dye. Among all samples, the film with 25 nm TiO_2 nanoparticles exhibited the highest specific surface area (78.2 m^2/g) and the greatest amount of dye adsorbed (2.81×10^{-8} mol/cm^2). It can be concluded that the optimal TiO_2 nanoparticle size of 25 nm enhances the specific surface area of the film structure, resulting in an increase in the amount of adsorbed dye.

Figure 6 shows the UV–Vis absorption spectra of TiO_2 thin films with different nanoparticle sizes of (a) 5, (b) 25, (c) 32, and (d) 100 nm before and after dye sensitization. The measurements

Table 1
BET surface area and amount of adsorbed dye on thin films with different nanoparticle sizes.

Sample	BET surface area (m^2/g)	Amount of dye in electrodes (10^{-8} mol/cm^2)
5 nm	65.4	2.43
25 nm	78.2	2.81
32 nm	58.9	2.17
100 nm	36.7	1.42

were performed in the wavelength range of 300–800 nm to evaluate the light absorption characteristics and dye adsorption efficiency of the films. For all samples, a significant increase in absorbance was observed after immersion in the N719 dye solution, especially in the range of 400–550 nm, which corresponds to the main absorption band of the N719 dye. Among all samples, the thin film doped with 25 nm nanoparticles [Fig. 6(b)] showed the highest increase in absorbance after dye loading, indicating its excellent dye adsorption capacity. This can be attributed to its good surface morphology and porosity (as shown in Figs. 4 and 5), which enhance the penetration of the dye and binding to the TiO_2 surface. The film with 100 nm nanoparticles [Fig. 6(d)] shows the lowest absorbance after dye sensitization, reflecting its poor dye loading capacity. As mentioned earlier, the low surface area and sparse film morphology reduce the number of adsorption sites available for dye molecules. These optical results are consistent with the microstructure and thickness analysis results of SEM images.

The photovoltaic performance of DSSCs fabricated with 5, 25, 32, and 100 nm nanoparticles is shown in Fig. 7 and Table 2. The *I–V* curves were measured under AM 1.5G simulated sunlight (100 mW/cm^2), and photovoltaic parameters were obtained from[23]

$$\eta = \frac{J_{sc} \times V_{oc} \times FF}{P_{in}}, \tag{1}$$

where V_{oc} is the open-circuit voltage (V), J_{sc} is the short-circuit current density (mA/cm^2), FF is the fill factor (%), η is the power conversion efficiency (%), and P_{in} is the incident light power density (100 mW/cm^2). Among all samples, the DSSC with 25 nm TiO_2 nanoparticles exhibited the best performance with J_{sc} of 14.49 mA/cm^2, V_{oc} of 0.69 V, a fill factor of 60.5%, and a maximum power conversion efficiency of 6.05 %. This performance is attributed to its optimized film morphology, high dye loading capacity, uniform grain connectivity, and high anatase phase. The 25 nm nanoparticle size provides the optimal surface area and crystalline phase, resulting in the best device performance.

To further analyze the spectral response, the incident photon-to-electron conversion efficiency (IPCE) spectra of all DSSCs are shown in Fig. 8. IPCE represents the wavelength-dependent efficiency of converting absorbed photons into collected electrons and is calculated as[24]

$$IPCE = \frac{1240 \times J_{sc}\left(\mathrm{mA/cm^2}\right)}{\lambda(\mathrm{nm}) \times I_{inc}\left(\mathrm{mW/m^2}\right)}, \tag{2}$$

where J_{sc} represents the photocurrent density in the short-circuit state and I_{inc} is the intensity of incident monochromatic light at a specific excitation wavelength λ. The IPCE spectra of all

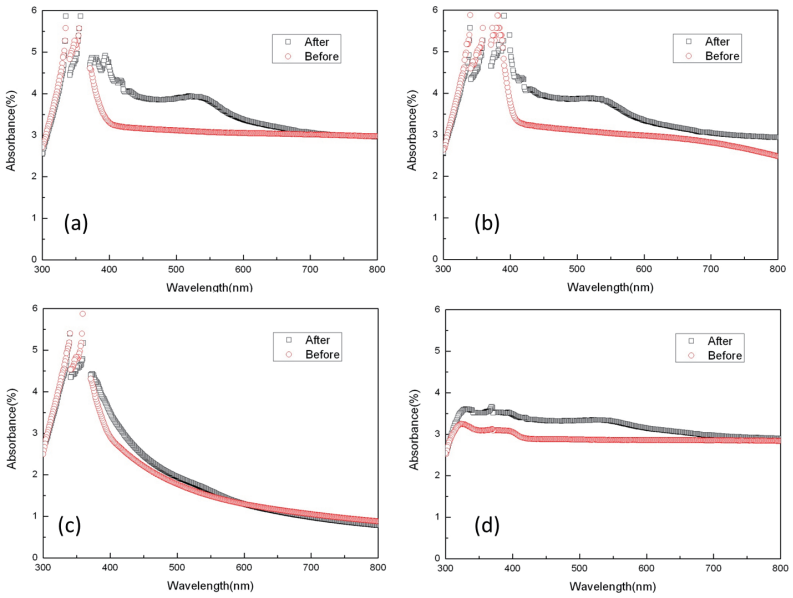

Fig. 6. (Color online) Absorbance spectra of TiO_2 thin films with nanoparticle sizes of (a) 5, (b) 25, (c) 32, and (d) 100 nm before and after immersion in dye.

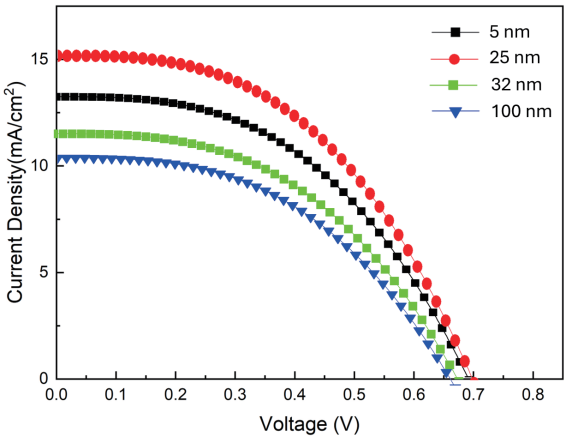

Fig. 7. (Color online) *I–V* curves of TiO_2 thin films with nanoparticle sizes of 5, 25, 32, and 100 nm.

Table 2
Photovoltaic performance of DSSCs using TiO_2 thin films with nanoparticle sizes of 5, 25, 32, and 100 nm.

DSSC	V_{oc} (V)	J_{sc} (mA/cm^2)	Fill factor (%)	η (%)
5 nm	0.68	12.76	59.5	5.16
25 nm	0.69	14.49	60.5	6.05
32 nm	0.66	11.52	58.2	4.42
100 nm	0.65	10.82	57.2	4.02

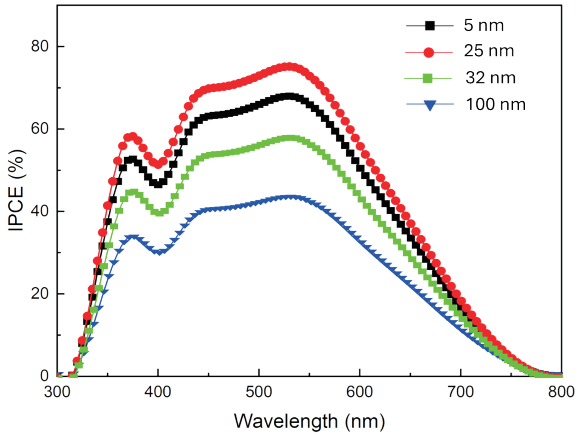

Fig. 8. (Color online) IPCE spectra of DSSC prepared using thin films with TiO_2 nanoparticle sizes of 5, 25, 32, and 100 nm.

samples show a characteristic broadband response from 350 to 750 nm, corresponding to the absorption curve of the N719 dye. The DSSC with 25 nm TiO_2 nanoparticles exhibits the highest IPCE in the entire wavelength range, reaching a peak of 80% around 530 nm. This enhanced performance is attributed to the optimized microstructure and high dye loading capacity characteristics of the film, which has been confirmed by previous SEM and UV–VIS results. The device fabricated with 100 nm nanoparticles has the lowest IPCE response, with a peak of about 40%. This indicates reductions in the amount of dye loaded and photon absorbed.

4. Conclusions

In this study, TiO_2 thin-film dye-sensitized solar cells were prepared by the sol–gel method and incorporated with TiO_2 nanoparticles of different particle sizes (5, 25, 32, and 100 nm). The effects of nanoparticle size on crystallinity, morphology, light absorptivity, and photovoltaic performance were studied. The results showed that TiO_2 thin films with 25 nm nanoparticles have a high anatase phase, high absorbance, and better dye adsorption capacity. The photovoltaic performance showed that the DSSC with 25 nm TiO_2 nanoparticles also showed the highest power conversion efficiency of 6.05 %. In addition, the IPCE of this DSSC also has an optimal value of about 80%. This is mainly attributed to the crystallization and morphology improved with the addition of 25 nm TiO_2 nanoparticles in the DSSC.

Acknowledgments

This work was sponsored by the National Science Council of the Republic of China under grant No. NSC 113-2637-E-324-001.

References

1 Y. Ahmadi, H. Teymourinia, S. Hosseininezhad, and A. Ramazani: Inorg. Chem. Commun. **162** (2024) 112153. https://doi.org/10.1016/j.inoche.2024.112153
2 A. Ashok, T. Raguram, R. J. Beula, G. Gopinath, S. Ayyasamy, and B. Vidhya: J. Alloys Compd. **1005** (2024) 176024. https://doi.org/10.1016/j.jallcom.2024.176024
3 A. Chaudhari, A. Kumar, S. Kumar, and S. Kushwaha: Mater. Res. Bull. **179** (2024) 112909. https://doi.org/10.1016/j.materresbull.2024.112909
4 H. C. Chen, J. Y. Li, and T. F. Liu: Opt. Mater. **143** (2023) 114292. https://doi.org/10.1016/j.optmat.2023.114292
5 M. Hosseinnezhad, K. Gharanjig, M. Ghahari, S. Nasiri, and M. Fathi: Sustain. Energy Technol. Assess. **72** (2024) 104066. https://doi.org/10.1016/j.seta.2024.104066
6 H. Kanwal, A. A. B. Khan, A. Al Ahmad, M. Ubaidullah, A. Shah, Z. Ali, T. Ghani, M. Younas, and M. Mehmood: Sol. Energy **282** (2024) 112952. https://doi.org/10.1016/j.solener.2024.112952
7 S. Mahalingam, R. Rabeya, A. Manap, K. S. Lau, C. H. Chia, N. Afandi, and A. Omar: Electrochim. Acta **510** (2025) 145369. https://doi.org/10.1016/j.electacta.2024.145369
8 M. Musharaf, M. Usman, N. Ahmed, and A. Shuja: Ceram. Int. **51** (2025) 28665. https://doi.org/10.1016/j.ceramint.2025.04.074
9 M. Onyemowo, Y. Unpaprom, and R. Ramaraj: Opt. Mater. **148** (2024) 114860. https://doi.org/10.1016/j.optmat.2024.114860
10 N. A. A. A. Rahman, A. Khasri, N. H. M. Salleh, M. R. M. Jamir, S. Ansar, R. Boopathy, and A. Syafiuddin: Desalin. Water Treat. **303** (2023) 151. https://doi.org/10.5004/dwt.2023.29791
11 N. Ravikumar, N. Pari, A. Kannan, J. K., and S. Gandhi: J. Power Sources **641** (2025) 236877. https://doi.org/10.1016/j.jpowsour.2025.236877
12 M. Yazdanipanah and M. R. Mohammadi: J. Photochem. Photobiol. A Chem. **467** (2025) 116418. https://doi.org/10.1016/j.jphotochem.2025.116418
13 M.-E. Yeoh, K.-Y. Chan, H.-Y. Wong, P.-L. Low, G. S. How Thien, Z.-N. Ng, H. C. Ananda Murthy, and R. Balachandran: Opt. Mater. **141** (2023) 113907. https://doi.org/10.1016/j.optmat.2023.113907
14 M. C. Kao, J.-H. Weng, C. H. Chiang, K. H. Chen, D. Y. Lin, and T. K. Kang: Energies **17** (2024) 5118. https://doi.org/10.3390/en17205118
15 M. C. Kao, H. Z. Chen, and S. L. Young: Jpn. J. Appl. Phys. **52** (2013) 01AD04. https://doi.org/10.7567/JJAP.52.01AD04
16 S. H. Yousef, E. Abdel-Latif, S. A. Badawy, and M. R. Elmorsy: RSC Adv. **15** (2025) 13896. https://doi.org/10.1039/d5ra00694e
17 V. Bhullar, S. Sardana, and A. Mahajan: Sol. Energy **230** (2021) 177. https://doi.org/10.1016/j.solener.2021.10.023
18 M.-E. Yeoh, K.-Y. Chan, H.-Y. Wong, G. S. H. Thien, P.-L. Low, Z.-N. Ng, H. C. A. Murthy, and R. Balachandran: Mater. Lett. **349** (2023) 134730. https://doi.org/10.1016/j.matlet.2023.134730
19 G. Fu, E. J. Cho, X. Luo, J. Cha, J. H. Kim, H. W. Lee, and S. H. Kim: Sol. Energy **218** (2021) 346. https://doi.org/10.1016/j.solener.2021.03.011
20 N. Ullah, S. M. Shah, R. Ansir, S. Erten-Ela, S. Mushtaq, and S. Zafar: Mater. Sci. Semicond. Process. **135** (2021) 106119. https://doi.org/10.1016/j.mssp.2021.106119
21 S. B. Wategaonkar, V. G. Parale, R. P. Pawar, S. S. Mali, C. K. Hong, R. R. Powar, A. V. Moholkar, H.-H. Park, B. M. Sargar, and R. K. Mane: Ceram. Int. **47** (2021) 25580. https://doi.org/10.1016/j.ceramint.2021.05.284
22 M. K. Hossain, A. A. Mortuza, S. K. Sen, M. K. Basher, M. W. Ashraf, S. Tayyaba, M. N. H. Mia, and M. J. Uddin: Optik **171** (2018) 507. https://doi.org/10.1016/j.ijleo.2018.05.032
23 M. C. Kao, H. Z. Chen, S. L. Young, C. C. Lin, and C. Y. Kung: Nanoscale Res. Lett. **7** (2012) 260. https://doi.org/10.1186/1556-276X-7-260
24 M. C. Kao, H. Z. Chen, and S. L. Young: Thin Solid Films **519** (2011) 3268. https://doi.org/10.1016/j.tsf.2010.12.032